Synthesis, characterization, and application of nano-perfluorooctyl alumina for adsorption of methyl tertiary-butyl ether (MTBE) from aqueous medium

Afshin Dehghani, Amanollah Ebadi*, Sirous Shafiei, Abbas Aghaeinejad-Meybodi

Chemical Engineering Department, Environmental Engineering Research Center, Sahand University of Technology, Tabriz, Iran, email: afshin_1982@ymail.com (A. Dehghani), Tel. +98 4133459140; Fax: +98 4133224950; emails: ebadi@sut.ac.ir (A. Ebadi), shafiei@sut.ac.ir (S. Shafiei), a.aghaei.meybodi@gmail.com (A. Aghaeinejad-Meybodi)

ABSTRACT

In this work, adsorptions of Methyl tertiary-butyl ether (MTBE) onto two novel adsorbents, i.e. nano-perfluorooctyl alumina was prepared using nano-γ-alumina (nano-PFOAL$_G$) and nano-boehmite (nano-PFOAL$_B$) as the supports were investigated. The surface areas of the nano-γ-alumina and nano-boehmite were determined as 265.7 and 319.5 m^2/g, respectively. The equilibrium adsorption behavior of the nanoadsorbents was studied for adsorption of (MTBE) in a wide range (100–1,750 mg/L) of aqueous phase concentrations. The maximum adsorption capacities were 46.0 and 44.4 mg MTBE/g adsorbent for nano-PFOAL$_G$ and nano-PFOAL$_B$, respectively. The Freundlich, Langmuir, and Brunauer–Emmet–Teller (BET) isotherms were used for modeling of MTBE adsorption on nano-PFOAL$_G$ and nano-PFOAL$_B$ from aqueous medium. The experimental results of MTBE adsorption on the surface of nano-PFOAL adsorbents obeyed a type IV van der Waals adsorption trend, which can be modeled best by the BET isotherm up to pore filling concentration.

Keywords: Adsorption; Nano-γ-alumina; Nano-perfluorooctyl alumina; MTBE; BET isotherm

1. Introduction

Methyl tertiary-butyl ether (MTBE) is used as an additive in gasoline formulation for enhancement of octane number and reduction of atmospheric pollutant emissions such as CO, NO$_X$, and unburnt hydrocarbons [1–4]. The quick transfer of MTBE from gasoline leaks to the surrounding water phase is due to MTBE's high solubility in water (about 50 g/L) and the low sorption of MTBE in soils. The MTBE distribution in the aqueous medium has raised concern about the compound's occurrence in drinking water, due to its low taste and odor threshold (20–40 µg/L, according to EPA's drinking water advisory) and the potential impact on human health. Different types of advanced oxidation processes (such as catalytic ozonation, photooxidation (UV/H$_2$O$_2$) and (UV/TiO$_2$)) are effective for MTBE removal from aqueous phase [5–7]. However, byproducts of the oxidation processes may remain in the treated water requiring a further removal step such as adsorption [8–11]. The adsorption process is one of the promising processes for the removal of MTBE from contaminated waters. Wieserman and Wefer used surface modification of alumina by perfluorinated organic molecules to develop sorbents for adsorption of organic materials [12]. Perfluorinated alumina (e.g. perfluorooctyl alumina) obtained by reaction between perfluorinated acids (e.g. perfluorooctanoic acid) and hydroxyl groups on the surface of
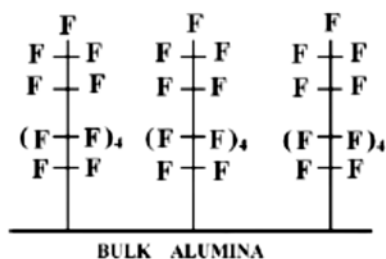
---

*Corresponding author.

Fig. 1. Schematic representation of perfluorooctyl groups on the surface of alumina [5].

alumina (Fig. 1). Since the perfluorinated groups that bonded on surface of alumina are hydrophobic and nonpolar, the organic pollutants in aqueous medium can be adsorbed by this modified surface. Kasprzyk-Hordern et al. used these types of adsorbents as novel ozonation catalysts for the removal of organic matters [13–19].

Also, they used perfluorinated alumina for adsorption of MTBE in the 0.2–38.0 mg/L range of aqueous phase concentrations [13]. In the previous work, conventional PFOAL samples were prepared and the adsorption capabilities of them were studied for removal of MTBE from aqueous phase [20]. Later, the mechanism and kinetics of the ozonation reactions were studied in the presence of conventional PFOAL [21].

In the present work, for enhancement of the adsorption capacity of PFOAL, an attempt was made for synthesis of nanoforms of PFOAL. The equilibrium adsorption behaviors of the adsorbents for MTBE were studied in a wide range of aqueous phase MTBE concentrations of 100–1,750 mg MTBE/L. The Freundlich, Langmuir, and Brunauer–Emmet–Teller (BET) isotherm models were used to model the adsorption trends of MTBE on the surface of the nano-PFOAL adsorbents.

2. Experimental

2.1. Chemicals

Aluminum nitrate ($Al(NO_3)_3 9H_2O$, purity $\geq$ 98%), sodium carbonate (Na_2CO_3, purity $\geq$ 99%), perfluorooctanoic acid ($CF_3(CF_2)_6COOH$, purity > 97%), ethanol (C_2H_5OH, purity $\geq$ 96%), acetone ($CO(CH_3)_2$, purity $\geq$ 99.7%), and sodium bicarbonate ($NaHCO_3$, purity $\geq$ 99.9%) were used for preparation of nano-perfluorooctyl alumina adsorbents (nano-$PFOAL_G$ and nano-$PFOAL_B$). Sodium chloride (NaCl, purity = 99.5%) was used to increase the extraction efficiency in the headspace analysis. Also, MTBE

$((CH_3)_3COCH_3$, purity $\geq$ 99%) solutions were used in adsorption experiments. All of the chemicals were purchased from Merck Company (Germany).

2.2. Synthesis of nanoadsorbents

For preparation nano-γ-alumina and nano-boehmite by co-precipitation method, aluminum nitrate, sodium carbonate and deionized water were used as starting chemicals. Initially, 400 mL of aluminum nitrate (0.041 M) and sodium carbonate (0.075 M) solutions were prepared. Then sodium carbonate and aluminum nitrate solutions were added drop by drop to 200 mL of deionized water in a 2 L capacity round-bottom flask and stirred well using magnetic stirrer (Labinco, Netherlands) to precipitate Al^{3+} cations in the form of hydroxides. The precipitate was aged at 70°C for 3 h, filtered and redispersed again in 2 L of hot deionized water. The precipitate was finally filtered, washed thoroughly with warm deionized water and subsequently with ethanol followed by acetone and air-dried at room temperature (25°C). The dried precipitates obtained from this stage were nano-boehmite that were calcined in a programmable furnace (Fine Tech, Korea) at 550°C for 5 h in air with heating rate of 2°C/min to produce nano-γ-alumina powders [22]. Two types of nano-perfluorooctyl alumina were synthesized with reaction between 10 g of supports (nano-γ-alumina or nano-boehmite) and 100 mL of 0.12 M perfluorooctanoic acid aqueous solution. In the preparation of PFOAL, perfluorooctanoic acid reacts with hydroxyl groups on the surface of γ-alumina or boehmite (see Fig. 1). The reaction mixture was kept at 60°C and stirred for 4 h. Then the solid was filtered, washed with 100 mL of 0.1 M sodium bicarbonate, then with 200 mL of H_2O, and dried at 60°C.

2.3. Characterization of nanoadsorbents

To identify the phases and the crystallinity of the calcined materials, X-ray diffraction (XRD) studies were carried out with a Siemens-D500 instrument. Specific surface areas of the nano-γ-alumina and nano-boehmite were determined by a ChemBET 3000 instrument (Quantochrome Industries) using physisorption of N_2 at its atmospheric boiling temperature. The surface morphology of synthesized particles was evaluated by scanning electron microscopy (SEM) using a VEGA II instrument. FT-IR analyses were performed for the supports, perfluorooctanoic acid and nano-PFOAL adsorbents by a Mattson 1000 FT-IR spectrometer. Elemental analyses of the samples were carried out using Perkin Elmer Series II instrument.

2.4. Analytical procedure

To obtain adsorption equilibrium isotherm data with the powdered adsorbents, aqueous phase adsorption experiments were performed in 10 mL glass vials using a fixed adsorbent/liquid ratio (0.1 g adsorbent/10 mL aqueous solution) and varied concentrations of MTBE initial solution (100, 300, 500, 750, 900, 1,000, 1,250, 1,500, and 1,750 mg/L). In all experiments, the vials were agitated on a fixed speed rotator for a minimum of 3 h at 160 rpm, for adsorption equilibrium to be achieved. Preliminary tests have also indicated that the time to reach the equilibrium was about 30 min. The adsorption amounts of MTBE in the samples were calculated according to Eq. (1).

$$q_e = \frac{(C_0 - C_{eq})V}{m_s} \tag{1}$$

where q_e is the equilibrium adsorption amount (mg/g), C_0 is the initial concentration of MTBE solution (mg/L), C_{eq} is the equilibrium concentration of MTBE solution (mg/L), V is the volume of solution (L), and m_s is the mass of adsorbent (g).

For measuring the MTBE concentrations in aqueous medium, a headspace injection method was employed using a gas chromatograph equipped with TRACE MS PLUS mass spectrometer (Thermo Finnigan, Italy). Separation was achieved by a DB1 (SGE) nonpolar capillary column (25 m, 0.22 mm, 0.25 μm). A constant temperature of 50°C for 8 min was used for the column oven. The injector temperature was 175°C. For quantitative analysis of the components of the reaction mixture, the selected ion monitoring (SIM) mode was used in the mass spectrometer detector. The mass number 73 were used for quantification of MTBE. Usage of SIM mode instead of full scanning mode makes it possible to avoid possible overlapping of the peaks of the various components. In this way one can obtain very sharp peaks, which can be used for more elaborate quantitative measurements. The carrier gas was helium with a flowrate of 0.5 mL/min in the column. The split mode was used in injector and split flowrate was 10 mL/min so the split ratio was 20. Sample injections were carried out using a 50-μL gastight syringe (Hamilton, Switzerland) and the injection volume was 25 μL. Under these conditions, the MTBE peak appeared at about 2.57 min retention time.

Careful considerations were applied in the analysis method by the GC/MS to reduce the possible errors. The GC/MS system was calibrated daily before starting the analysis of the samples. Also for showing the repeatability of the analysis results, each sample was analyzed more than three times (3–5 times). The relative standard deviation for the results of a sample was less than 3%.

2.5. Isotherm models

2.5.1. Freundlich isotherm

This is an empirical isotherm which implies a logarithmic reduction in heat of adsorption by increasing the amount adsorbed on the solid surface [23]. It is a general and versatile model expressed as Eq. (2).

$$q = KC_{eq}^{\eta} \tag{2}$$

where C_{eq} is the equilibrium concentration of the adsorbents in fluid phase and q is the amount adsorbed on solid surface. The empirical exp η and the constant K are determined by fitting the model equation to the experimental adsorption data.

2.5.2. Langmuir isotherm

Langmuir isotherm has a great general utility. In the development of this model a monolayer adsorption was assumed and so the entire amount adsorbed experimentally is considered as the monolayer adsorption. Despite its simplifying assumptions which may seem unrealistic in most of applications, it has a great popularity mainly because of its simple form and reasonably good prediction. Eq. (3) presents a general form of Langmuir isotherm [24]:

$$q = q_m \frac{K_S C_{eq}}{1 + K_S C_{eq}} \tag{3}$$

In Eq. (3), q_m is the amount adsorbed on complete monolayer adsorption or in other words the maximum amount adsorbed. K_S is the equilibrium constant of adsorption. These parameters are determined by fitting the model equation to the experimental data.

2.5.3. BET multilayer adsorption isotherm

The first version of the BET multilayer isotherm as Eq. (4) was originally developed in 1938 for gas phase adsorption [25]. It could only describe types II and III of van der Waals adsorption isotherms [23].

$$q = q_m \frac{cx}{(1-x)(1-x+cx)} \tag{4}$$

where x is the relative partial pressure of the adsorbate in bulk gas phase, i.e. $x = P/P^S$ and c is a constant. This equation has two degrees of freedom of q_m and c, which are determined by numerical regression using experimental data.

By a close examination of derivation of BET isotherm, it was showed that when extending application of this equation to liquid phase adsorption, $x = K_L C_{eq}$ and $c = K_S/K_L$. So the BET equation for liquid phase adsorption should be written in the form of Eq. (5) [26]:

$$q = q_m \frac{K_S C_{eq}}{(1 - K_L C_{eq})(1 - K_L C_{eq} + K_S C_{eq})} \qquad (5)$$

In Eq. (5) K_S is the equilibrium constant of adsorption of the first layer and K_L is the equilibrium constant of adsorption for upper layers of adsorbate on the adsorbent. This form of BET equation for liquid phase adsorption has three degrees of freedom of q_m, K_S, and K_L, which need to be determined from experimental data.

3. Results and discussion

3.1. Syntheses and characterization of nanoadsorbents

A transparent gel-like precursor containing Al cations was precipitated at pH ~7.5–8.5 when sodium carbonate and aluminum nitrate solutions were added drop by drop to 200 mL deionized water. The mixture was stirred and maintained at a temperature of 70°C. The following chemical reactions occurred:

$$Na_2CO_3 + 2HOH \rightarrow 2NaOH + H_2O + CO_2 \qquad (6)$$

$$Al(NO_3)_3 + 3NaOH \rightarrow Al(OH)_3 \downarrow + 3NaNO_3 \qquad (7)$$

The hydrolysis of sodium carbonate in aqueous medium generates OH^- ions by reaction (6). The precipitate obtained by reaction (7) was aged at a temperature ~70°C, which helped to homogenize it due to the slow ripening process. The precipitate was further processed by washing with deionized water first, followed by washing with alcohol and acetone to avoid the contamination of sodium ions. The digestion step is found to be essential to convert it to crystalline boehmite precursor by reaction (8). nano-γ-alumina was produced by calcination of dried nano-boehmite at 550°C by reaction (9) [22].

$$Al(OH)_3 \rightarrow AlOOH + H_2O \qquad (8)$$

$$AlOOH \rightarrow Al_2O_3 + H_2O \qquad (9)$$

3.1.1. X-ray diffraction

The XRD studies were taken on as-dried precursor and calcined samples. Fig. 2 shows the XRD patterns of the boehmite and γ-alumina, respectively. All the reflections of boehmite synthesized by co-precipitation method at 70°C matched with pattern of boehmite according to [JCPDS File No. 21-1307]. The intensity of XRD peaks is dependent on phase content, crystallinity degree, and its crystal size that the sharp peaks with high intensity indicated high crystallinity of the samples. The boehmite prepared at 70°C appears to be crystalline in nature. It seems that precipitation for 3 h helps to generate crystalline boehmite due to a fast ripening process, as explained by Potdar et al. [22]. It is very obvious from broad peaks in Fig. 2(a) that the boehmite precursor particles show nano-sized nature and also indicate presence of small crystallite sizes in sample. The crystallite sizes were calculated using the Scherrer equation [27]:

$$D = \frac{k\lambda}{\beta \cos \theta} \qquad (10)$$

where k is a constant ~0.9, λ is the wave length of the X-rays, β is the full width of diffraction peak at half maximum intensity, and θ is the Bragg angle. The calculated crystallite sizes were found to be in the range of 1.5–2.5 nm. It is established [27–31] that conversion of aluminum hydroxide to single-phase
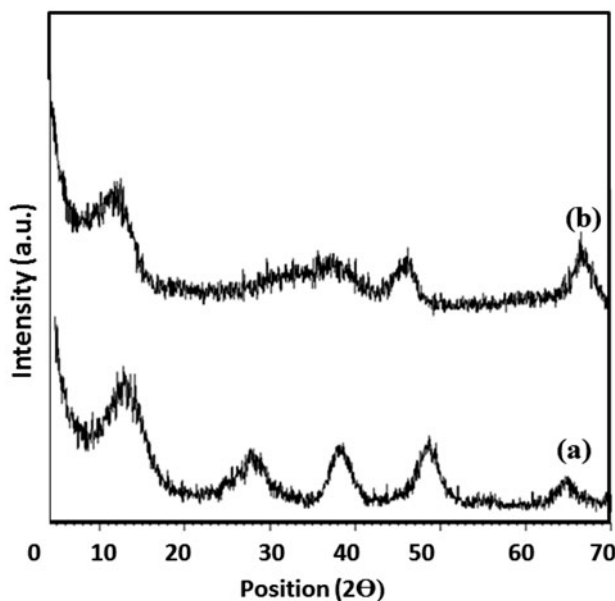
Fig. 2. XRD pattern of (a) nano-boehmite and (b) nano-γ-alumina.

nano-boehmite is dependent on many parameters such as temperature, nature of base, and type of aluminum salt. The present results showed that co-precipitation at 70°C was able to produce nano-boehmite with high purity.

Fig. 2(b) shows the XRD pattern of samples prepared after calcination of boehmite at 550°C in air. All XRD peaks of the calcined sample are exactly indexed to γ-alumina and no clear peaks from other phases of alumina are observed. Also Fig. 2(b) indicates that the γ-alumina phase having spinel lattice [JCPDS File No. 29-63] and pure crystalline in nature [27]. The broadening of the XRD peaks displayed the nano-sized nature of γ-Al_2O_3 particles in these samples. The crystallite sizes calculated using the Scherrer equation were found to be in the range of 2.5–3 nm. The formation of crystalline nano-boehmite and nano-γ-alumina in the co-precipitation process were confirmed by XRD pattern of the samples.

3.1.2. Scanning electron microscopy

Morphologies of nano-boehmite and nano-γ-alumina observed by SEM are shown in Figs. 3 and 4 in two different scales. The nano-boehmite and nano-γ-alumina indicated strong agglomeration of particles with varied sizes. Because of the high surface area of the nano-boehmite samples, the surface area has a high tendency to decrease during the calcination of nano-boehmite. This abatement of the surface area is a result of the formation of strong bonds in contact regions of nano-γ-alumina particles with diffusion mechanism, and consequently results in stronger and greater agglomeration in nano-γ-alumina. The agglomeration is mainly caused by the absorbed water and the surface hydroxyl groups in the precipitated hydroxide along with the particle agglomeration occurring when the precipitated precursors with small size are dried and calcined.

3.1.3. Brunauer, Emmett, and Teller analysis

The nano-boehmite and nano-γ-alumina powder showed similar morphological features. The surface area, pore size distribution, and pore volume data obtained for boehmite and nano-γ-alumina powder are tabulated in Table 1, which shows that nano-boehmite has a larger surface area. More importantly, surface area obtained for these samples are very high compared with commercial conventional alumina samples. At least more than 100 m^2/g surface areas are needed for PFOAL adsorbents to have sufficient and more enough adsorption capacities [12–19].

3.1.4. Fourier transforms infrared spectroscopy (FT-IR)

The FT-IR spectra of nano-boehmite, nano-γ-alumina, perfluorooctanoic acid, and nano-PFOAL adsorbents are presented in Fig. 5. FT-IR spectra of nano-boehmite and nano-γ-alumina show a broad band around 3,447 and 1,640 cm^{-1}, which is assigned to stretching and bending modes of adsorbed water. The peak corresponding to 1,073 cm^{-1} is assigned to Al–O–Al symmetric bending stretching vibrations and that around 1,160 cm^{-1} is due to asymmetric bending modes. The bands at 480 and 617 cm^{-1} are attributable
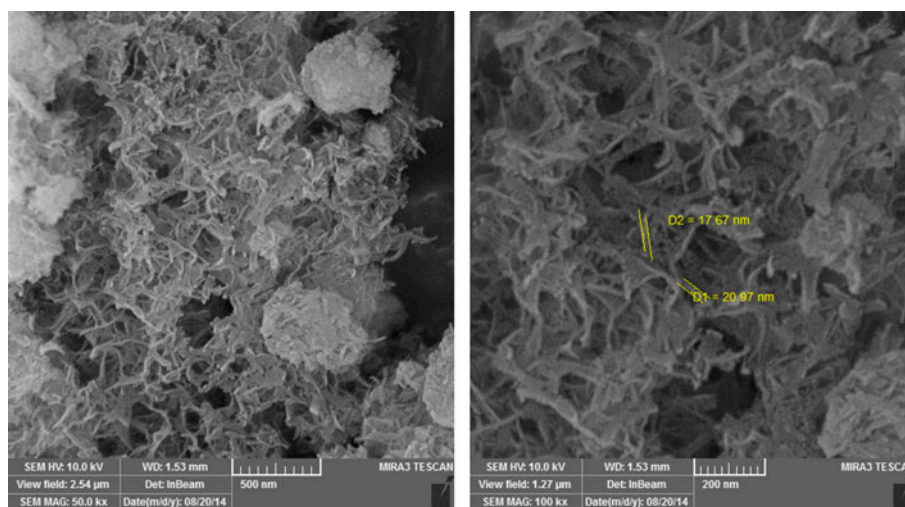

Fig. 3. SEM photographs of the nano-boehmite powder.

Fig. 4. SEM photographs of the nano-γ-alumina powder.

Table 1
Surface area, pore size distribution, and pore volume of nano-boehmite and nano-γ-alumina

Sample	Synthesis method	Surface area (m^2/g)	Average pore diameter (nm)	Pore volume (cm^3/g)
nano-boehmite	Co-precipitation	319.53	3.72	0.201
nano-γ-alumina	Co-precipitation	265.69	5.14	0.270

Fig. 5. IR spectra of (a) nano-boehmite, (b) nano-γ-alumina, (c) nano-PFOAL$_G$, (d) nano-PFOAL$_B$ and (e) perfluorooctanoic acid.

to bending and stretching modes of AlO_6. Peak at $750\ cm^{-1}$ may be due to Al–O stretching vibrations. Thus, the IR analysis of as-dried precursor confirmed that the nano-boehmite is formed by reaction (8). In the spectrum of calcined powder shown in Fig. 5, the peaks in the region of 500–$750\ cm^{-1}$ are assigned to υ-AlO_6, whereas the shoulder at 890 and the line at $800\ cm^{-1}$ are assigned to υ-AlO_4. Thus, γ-alumina phase contains both tetrahedral and octahedral coordination. The broad band at $3,447\ cm^{-1}$ and the weak band at $1,640\ cm^{-1}$ are due to adsorbed water [22]. Intense sharp bands at $1,155$ and $1,209\ cm^{-1}$ in the FT-IR spectrum of perfluorooctanoic acid can be attributed to C–F stretching vibrations. The band at $1,719\ cm^{-1}$ indicates C=O stretching vibrations for carboxylic acids. The weak bands at $2,490\ cm^{-1}$ represent O–H group of carboxylic acid. There are bands responsible for C–C vibrations in the wave number range of 700–$1,500\ cm^{-1}$. In the spectra of nano-PFOAL adsorbents there is a sharp band at $1,680\ cm^{-1}$, which can be attributed to C=O stretching vibrations. This suggests that bonding of perfluorooctanoic acid proceeds via COOH group interactions with OH groups on the alumina surface. The bands at $1,155$ and $1,209\ cm^{-1}$ observed in the spectra of perfluorooctanoic acid are also present in the spectra of

the nano-PFOAL adsorbents, which confirms the interaction of perfluorooctanoic acid with the surface of the supports. The weak band at 2,490 cm^{-1}, indicating the presence of the OH group of the carboxylic acid in perfluorooctanoic acid is shifted to 2,390 cm^{-1} in the spectra of the nano-PFOAL adsorbents. FT-IR spectra of the prepared nano-PFOAL adsorbents confirm that the perfluorooctanoic acid reacted effectively with the OH groups on the surface of the supports and that the per-fluorooctyl groups were bonded to the surface.

3.1.5. Elemental analysis (CHNOS)

The results of the elemental analysis (CHNOS) of the nano-boehmite and nano-γ-alumina supports and the prepared nano-PFOAL adsorbents are shown in Table 2.

The calculated surface coverage, perfluorinated phase content, and surface area of the nano-PFOAL adsorbents are shown in Table 3.

The surface coverage and perfluorinated phase content of the nano-PFOAL adsorbents are calculated using their carbon content determined by the elemental analysis and the surface areas of the nano-PFOAL adsorbents were calculated by considering their alumina (support) content. The surface areas of the alumina supports were determined by BET method and were given in Table 1.

The results of the characterization analyses showed that the surface areas of the prepared nano-PFOAL adsorbents are about two times more than that of conventional PFOAL adsorbents [12–19], but the surface coverage per unit area of the present nano-PFOAL adsorbents are somewhat lower than that of the conventional ones. The reason for the lower surface coverage of the present nano-PFOAL adsorbents in comparison to the conventional PFOAL adsorbents may be because of two reasons. First, the lower surface concentration of OH groups on the surface of the nano-boehmite and nano-γ-alumina, and second may be the lower average pore sizes of the present alumina supports because the perfluoroctanoic acid molecules cannot enter pores smaller than 12.5 Å (the kinetic diameter of perfluorooctanoic acid molecules that estimated using bond lengths between adjacent atoms [32]) to react with their surface. A possible solution

Table 2
Elemental analysis of the boehmite and nano-γ-alumina supports and nano-PFOAL adsorbents

Sample	Synthesis	C (%)	H (%)	N (%)
nano-PFOAL$_G$	Wieserman	6.18	1.07	0.06
nano-PFOAL$_B$	Wieserman	6.46	2.05	0.08
nano-boehmite	Co-precipitation	0.48	2.92	0.22
nano-γ-alumina	Co-precipitation	0.38	1.64	0.20

for modifying the surface of small pores may be the use of perfluoro acids with smaller molecular sizes, e.g. perfluoro acetic acid. Nevertheless, because of the higher surface areas of the supports, the perfluorooctyl content of the present nano-PFOAL adsorbents are very high compared with the conventional PFOAL adsorbents prepared by conventional alumina supports [12–19]. These higher perfluorooctyl contents can result in high adsorption capacities and also higher catalytic efficiency for ozonation reactions.

3.2. Adsorption of MTBE on the nano-perfluorooctyl alumina adsorbents

Experimental data of the adsorption of MTBE on the nanoadsorbents, PFOAL$_G$ and PFOAL$_B$, are shown in Figs. 6 and 7. These experimental data showed that nano-PFOAL adsorbents have considerable adsorption capacity for adsorption of MTBE, whereas the results of the adsorption experiments on nano-γ-alumina and nano-boehmite supports showed that MTBE did not adsorb on this supports. As shown in Figs. 6 and 7, the amount of MTBE adsorbed by the nano-PFOAL adsorbents increased by increase in liquid phase MTBE concentration and also the maximum adsorption capacities of nano-PFOAL$_G$ and nano-PFOAL$_B$, which occur at high aqueous phase concentrations, were 46.0 and 44.4 mg MTBE/g adsorbent, respectively, but above of these values, amount of MTBE adsorption did not increase with change in MTBE concentration in aqueous medium. This may be explained by the pore-filling phenomenon that occurred at high liquid phase concentration.

The Freundlich, Langmuir, and BET isotherm models are used to model the adsorption trend of MTBE on the nano-PFOAL adsorbents, and the results are shown in Figs. 6 and 7.

Table 3
Surface coverage, perfluorinated phase content, and surface area of the nano-PFOAL adsorbents

Sample	Surface coverage (μmol/m^2)	Perfluorinated phase content (μmol/g)	Surface area (m^2/g)
nano-PFOAL$_G$	2.94	604	204.85
nano-PFOAL$_B$	2.55	622	244.09

Table 4 shows the calculated parameters for these adsorption isotherm models applied to the results of adsorption experiments of MTBE on the nano-PFOAL adsorbents.
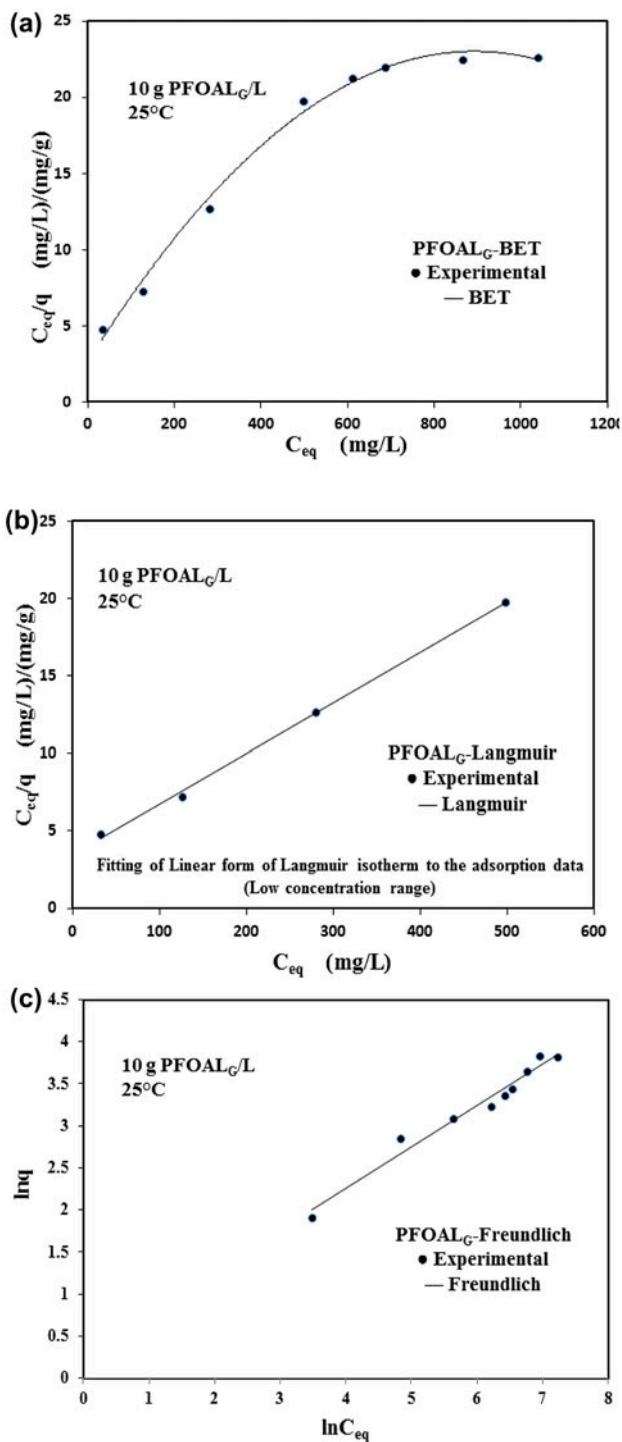

Fig. 6. Comparison of experimental data and performance of isotherm models in aqueous phase adsorption of MTBE on nano-PFOAL$_G$: (a) BET, (b) Langmuir, and (c) Freundlich isotherms.
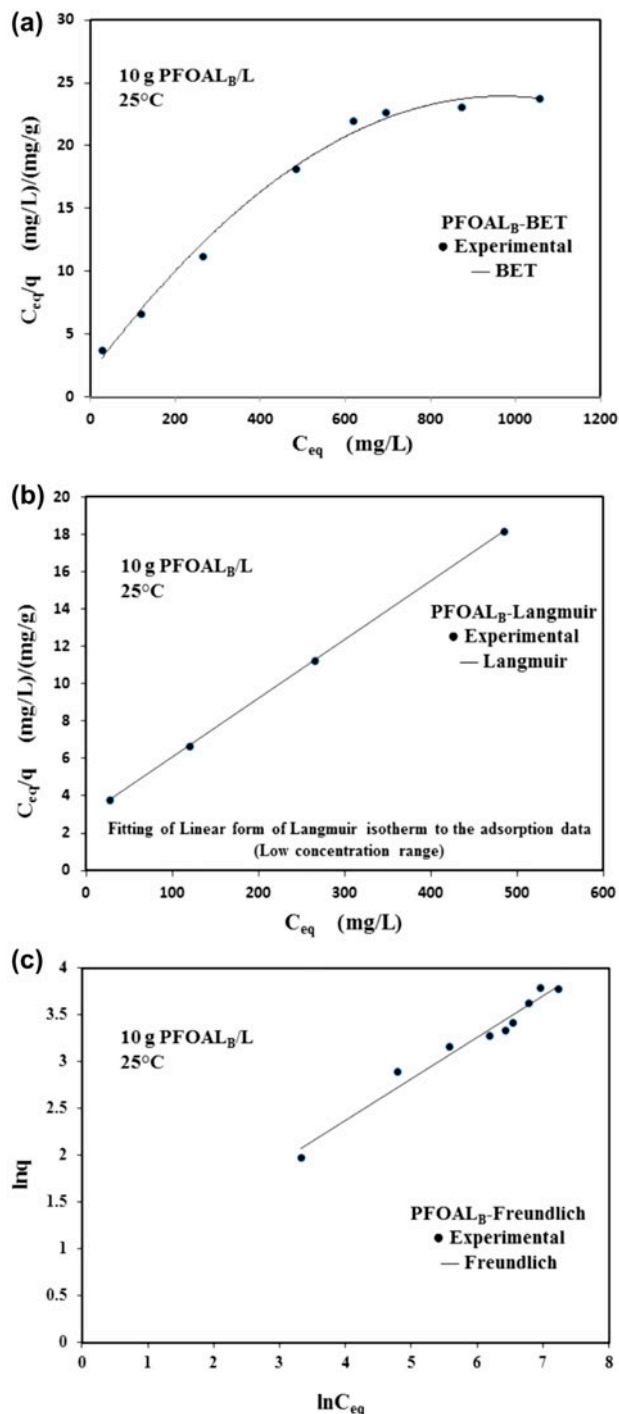
Fig. 7. Comparison of experimental data and performance of Isotherm models in aqueous phase adsorption of MTBE on nano-PFOAL$_B$: (a) BET, (b) Langmuir, and (c) Freundlich isotherms.

Table 4
Calculated parameters of the isotherm models for adsorption of MTBE on nano-PFOAL adsorbents

Isotherm model	Parameter	nano-PFOAL$_G$	nano-PFOAL$_B$
Freundlich	K (mg/g) (mg/L)$^{-\eta}$	1.324	1.8334
	η	0.493	0.442
	R^2	0.970	0.968
Langmuir (low concentration range)	K_S (mg/L)$^{-1}$	0.00933	0.01087
	q_m (mg/g)	30.65	31.69
	R^2	0.998	0.999
BET	K_S (mg/L)$^{-1}$	0.01853	0.0256
	K_L (mg/L)$^{-1}$	0.000543	0.000505
	q_m (mg/g)	20.61	21.09
	R^2	0.993	0.992

Table 5 shows the relative deviations of the amount of MTBE adsorption on the nano-PFOAL adsorbents with the prediction by isotherm models at different liquid phase concentrations.

Figs. 6 and 7 showed obviously that among the applied isotherms for adsorption of MTBE on the nano-PFOAL adsorbents, the BET isotherm can model the experimental data up to medium concentration range (up to pore-filling concentration). The correlation coefficient (R^2) (Table 4) and relative deviations of the regression calculations for the isotherm models (Table 5) confirm the above claim. Also the BET iso-

therm can model the S-shaped trend of experimental data. The experimental results of MTBE adsorption on these nanoadsorbents at whole concentration range obeyed a type IV van der Waals adsorption trend, which can be modeled better by BDDT isotherm (more general form of BET isotherm). Because of the complex form of BDDT isotherm it was not used here.

In comparison with the BET isotherm, Langmuir and Freundlich isotherms cannot model the experimental data of adsorption of MTBE on nanoadsorbents admirably in the wide range of MTBE concentrations. As shown in Table 5, the relative deviations for

Table 5
Relative deviations of the amount of adsorption of MTBE on nano-PFOAL adsorbents with prediction by isotherm models at different liquid phase concentrations

C_0 (mg/L)	C_{eq} (mg/L)	q (mg/g)	% Deviation = 100 $(q_{calc} - q)/q$		
			Freundlich	Langmuir	BET
nano-PFOAL$_G$					
1,750	1,296.0	45.4	−0.02	−37.6	–
1,500	1,039.8	46.0	−11.4	−39.6	0.58
1,250	865.0	38.5	−3.3	−29.1	−2.2
1,000	687.5	31.2	6.2	−15.1	0.32
900	611.9	28.8	8.8	−9.4	1.1
750	498.1	25.1	12.4	16.0	3.9
500	279.6	22.0	−3.2	0.56	−5.2
300	126.3	17.3	−17.0	−4.5	−8.8
100	32.4	6.7	8.9	5.29	17.7
nano-PFOAL$_B$					
1,750	1,311.0	43.9	0.3	−32.5	–
1,500	1,064.8	44.4	−9.9	−34.3	−0.004
1,250	883.1	37.8	−2.7	−24.1	−2.7
1,000	699.0	30.5	8.6	−8.5	2.4
900	611.5	28.1	12.1	−1.9	4.4
750	483.8	26.6	6.4	0.04	−1.1
500	264.7	23.5	−7.8	−0.03	−8.2
300	119.9	18.0	−15.2	−0.04	−4.5
100	27.5	7.2	9.7	0.6	22.9

these isotherm models are higher than BET isotherm. Although comparison of performance of the Freundlich isotherm and experimental data was better than the Langmuir isotherm in the whole range of MTBE concentrations, but as shown in part b of Figs. 6 and 7, Langmuir isotherm showed preferable performance at low concentration ranges. This is an expected result for Langmuir isotherm, because Langmuir isotherm cannot consider multilayer adsorption phenomenon. In Langmuir isotherm, all of the observed adsorption is considered as monolayer adsorption. Therefore, at concentrations less than the concentration at which monolayer adsorption completes, the relative deviations for these isotherm models are very low. Also for above reason the calculated monolayer adsorption capacity, q_m, predicted by Langmuir isotherm is much higher than the value of q_m calculated by the BET isotherm (see Table 4).

The BET isotherm provides a conceptual insight to the physical nature of the adsorption process on the surface of nano-PFOAL adsorbents, whereas the Freundlich and Langmuir isotherms may be more convenient for engineering calculations.

As shown in Table 4, the monolayer adsorption capacities, q_m, of nano-PFOAL$_G$ and nano-PFOAL$_B$ adsorbents isotherm are 20.6 and 21.1 mg MTBE/g adsorbent, respectively. Kasprzyk-Hordern et al. reported that the Langmuir isotherm could model the adsorption of MTBE [13] at low ranges of liquid phase concentrations, i.e. 0.2–38.0 mg/L. In this range of concentrations, less than a monolayer of MTBE can be adsorbed on the solid surface and the application of the Langmuir isotherm is justified. In this work, a wide range of liquid phase concentrations was investigated, i.e. 100–1,750 mg/L, and the Langmuir isotherm could not model the entire concentration range appropriately. This result was also obtained in our previous work that a wide range of liquid phase concentrations was investigated, i.e. 5–1,000 mg/L. The adsorption capacity of the nano-PFOAL$_B$ at low concentration ranges, i.e. its monolayer adsorption capacity, was slightly higher than that of nano-PFOAL$_G$, i.e. 21.1 vs. 20.6 mg MTBE/g adsorbent. This is because of its slightly higher perfluorinated phase content, i.e. 622 vs. 604 µmol/g. However, the total adsorption capacity of nano-PFOAL$_G$ is higher than nano-PFOAL$_B$, i.e. 46.0 vs. 44.4 mg MTBE/g adsorbent, in spite of its lower perfluorinated phase content, i.e. 604 vs. 622 µmol/g. This may be due to the fact that nano-PFOAL$_G$ has a larger average pore size and can adsorb more layers of MTBE on the surface of its larger pores. As shown in Figs. 6 and 7, the adsorption behaviors of nano-PFOAL$_G$ and nano-PFOAL$_B$ are very similar and only differ at high liquid concentra-

tions where the pores are somewhat more packed with adsorbed layers of MTBE. These results show that the pore-filling mechanism dominates at high concentration range, while at low concentrations the adsorption is directly related to hydrophobic characteristics of the surface.

Adsorption isotherms of MTBE on nano-PFOAL$_G$ at various temperatures (288, 298, 308, and 318 K) of solution are shown in Fig. 8. As shown in this figure, the adsorption amount decreased by increasing temperature which is a common trend in adsorption processes. The adsorption process confirms the BET adsorption isotherm to high correlation coefficient (>0.99). Values of BET parameters, q_m, K_L, and K_S for different temperatures are given in Table 6. It is clear that the complete monolayer adsorption amount (q_m) was nearly constant vs. temperature and varies only within the range of experimental errors.

Fig. 9 shows the efficiency of MTBE removal from water by nano-PFOAL adsorbents. The removal efficiency can be calculated as

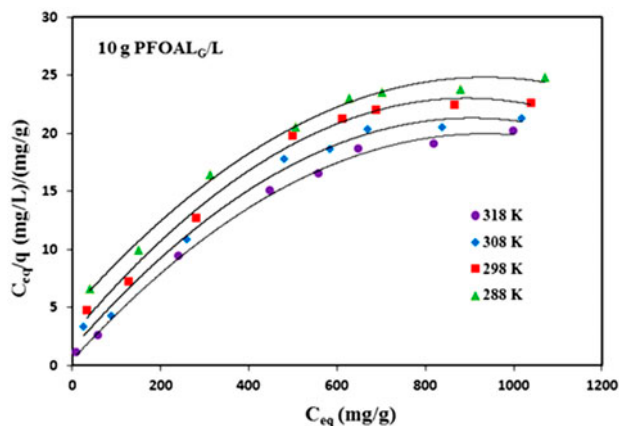$$\text{Removal efficiency} = \frac{(C_0 - C_{eq})}{C_0} \times 100 \tag{11}$$

Fig. 8. Adsorption of MTBE on nano-PFOAL$_G$ at various temperatures fitted by BET isotherm equation.

Table 6
BET adsorption isotherm constants at different temperatures

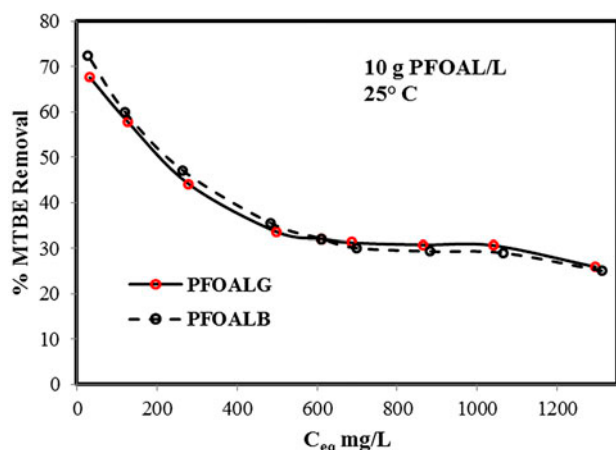| T (K)	K_L (mg/L)$^{-1}$	K_S (mg/L)$^{-1}$	q_m (mg/g)	(R^2)
288	0.000517	0.00905	19.90	0.993
298	0.000543	0.01853	20.61	0.993
308	0.000572	0.00985	21.09	0.991
318	0.000591	0.01451	21.44	0.997

Fig. 9. Percentage of MTBE removed from water by nano-PFOAL adsorbents at different equilibrium concentrations (% Removal = $(C_0 - C_{eq})/C_0$).

where C_0 and C_{eq} are the initial and equilibrium concentration of MTBE in the aqueous phase, respectively. At low concentrations, i.e. ~30 mg MTBE/L, the MTBE removal efficiency using 10 g nano-PFOAL/L was more than 67%. But as the aqueous phase concentration increased, the removal efficiency decreased and at high concentrations, i.e. ~1,300 mg MTBE/L, the MTBE removal efficiency is only about 25%. A comparison of the removal efficiency of MTBE by these two adsorbents supports the discussions above. At lower liquid phase concentrations, the removal efficiency by nano-PFOAL$_B$ is higher than that of nano-PFOAL$_G$ because its perfluorinated phase content is higher than nano-PFOAL$_G$, i.e. 622 vs. 604 μmol/g but at the higher concentration range the removal efficiency by nano-PFOAL$_G$ is greater, since its average pore size is larger than that of nano-PFOAL$_B$. Beyond the saturation concentration for the two adsorbents, i.e. 1,050 mg/L, the removal efficiency is equal for both of them.

Table 7
Active surface area of the nano-PFOAL adsorbents for adsorption of MTBE

		nano-PFOAL$_G$	nano-PFOAL$_B$
q_m	mg MTBE/g	20.61	21.09
q_m	μmol MTBE/g	233	239
S_{MTBE}	m^2/g	46.7	47.8

Active surface areas of the nanoadsorbents calculated by using of the monolayer adsorption capacity for MTBE are shown in Table 7. This is the active surface area of the nanoadsorbents for MTBE adsorption.

The active surface areas of the nanoadsorbents that can adsorb MTBE molecules are in very good agreement with their perfluorinated phase content. A comparison of the surface areas of nanoadsorbents occupied by adsorbed MTBE, with the total surface areas of nano-γ-alumina and nano-boehmite as supports determined by BET analysis, shows that as expected, only a small portion of the total surface area of the supports was occupied by adsorbed MTBE molecules. This is due to the fact that MTBE was only adsorbed on the regions that were initially covered by perfluorooctyl chains, i.e. MTBE did not adsorb on the bare surface of the alumina. This fact has been confirmed by separate adsorption experiments conducted using bare supports, which showed no adsorption of MTBE. This leads to the conclusion that the surfaces of the small pores which could not be modified by perfluorooctanoic acid (because of spatial hindering) would not adsorb MTBE molecules.

The synthesis of PFOAL adsorbents in nanoscale increased the surface area and perfluorinated phase content of this type of adsorbents.

The monolayer adsorption capacities of the prepared nano-PFOAL adsorbents were 20.6 and 21.1 mg

Table 8
The adsorption capacity of MTBE for various adsorbents

Adsorbent	Temperature (K)	Maximum adsorption capacity (mg/g)	Ref.
Granular activated carbon	301	204.1	[33]
Surfactant modified zeolite (SMZ)	293	100	[34]
Zeolite composites (silicalite-1/fly ash cenosphere)	298	92.5	[35]
Zeolite composite (silicalite-1/diatomite)	298	48.4	[35]
Ambersorb 572 resin	291	4.61	[36]
Ambersorb 563 resin	291	4.38	[36]
Mordenite zeolite	291	2.71	[36]
F400 carbon	291	1.41	[36]
nano-PFOAL$_G$	298	46	This work
nano-PFOAL$_B$	298	44.4	This work

MTBE/g PFOAL and the maximum adsorption capacities were 46.0 and 44.4 mg MTBE/g PFOAL for nano-PFOAL$_G$ and nano-PFOAL$_B$, respectively. These are about seven times higher than that of conventional PFOAL adsorbents in a previous work [20]. The reason for these considerably higher adsorption capacities is the increase in both the surface area and the perfluorinated phase content of the nano-perfluorooctyl alumina adsorbents in comparison with the conventional PFOAL adsorbents.

In order to compare the adsorption capacities of nano-PFOAL adsorbents with other adsorbents, the adsorption capacities of some other adsorbents for MTBE are given in Table 8. According to this table, the adsorption capacities of the synthesized nano-PFOALs adsorbents (44.4 and 46 mg/g) are comparable with the adsorption capacity of zeolite composite adsorbent (48.4 mg/g) and also are higher than adsorbents such as Ambersorb resins.

4. Conclusions

Two types of nano-PFOAL adsorbents, designated as nano-PFOAL$_B$ and nano-PFOAL$_G$, were used for the adsorption of MTBE. These adsorbents were prepared using nano-boehmite and nano-γ-alumina as the supports, respectively. The surface area of nano-γ-alumina and nano-boehmite supports were 265.7 and 319.5 m^2/g and their crystallite size obtained from XRD analyses and Scherrer equation were 2.5–3 and 1.5–2.5 nm, respectively. The surface coverage of the nano-PFOAL adsorbents by perfluorooctyl groups were 2.55 and 2.94 μmol/m^2 and perfluorinated phase content 622 and 604 μmol/g, respectively, for nano-PFOAL$_B$ and nano-PFOAL$_G$. The adsorption capacities of the synthesized nano-PFOAL adsorbents were very high in comparison with the adsorption capacity of conventional PFOAL adsorbents. This is due to increase in the surface area and perfluorinated phase content of the nano-PFOAL adsorbents. For example, the monolayer adsorption capacities of the prepared nano-PFOAL adsorbents were 20.6 and 21.1 mg MTBE/g PFOAL and the maximum adsorption capacities were 46.0 and 44.4 mg MTBE/g PFOAL for nano-PFOAL$_G$ and nano-PFOAL$_B$, respectively. These are about seven times higher than that of conventional PFOAL adsorbents. This shows that the monolayer adsorption capacity depends on the perfluorinated phase content of the adsorbents, while the maximum adsorption capacity is limited by the pore size of the adsorbent. At high concentration ranges, a pore-filling mechanism dominates the adsorption, while at low concentrations the adsorption can be correlated by the hydrophobic character of the surface.

References

[1] R. Pozzi, F. Pinelli, P. Bocchini, G.C. Galletti, Rapid determination of methyl tert-butyl ether using dynamic headspace/ion mobility spectrometry, Anal. Chim. Acta 504 (2004) 313–317.

[2] H. Borsdorf, A. Rammler, Continuous on-line determination of methyl tert-butyl ether in water dynamic headspace/ion mobility spectrometry, J. Chromatogr. 2005 (1072) 45–54.

[3] A. Kolb, W. Püttmann, Methyl tert-butyl ether (MTBE) in snow samples in Germany, Atmos. Environ. 40 (2006) 76–86.

[4] L.T. Hsieh, H.H. Yang, Ambient BTEX and MTBE in the neighborhoods of different industrial parks in Southern Taiwan, J. Hazard. Mater. 128 (2006) 106–115.

[5] B.S. Tawabini, Simultaneous removal of MTBE and benzene from contaminated groundwater using ultraviolet-based ozone and hydrogen peroxide, Int. J. Photoenergy 2014 (2014) 1–7, doi: 10.1155/2014/452356.

[6] Bassam S. Tawabini, Removal of methyl tertiary butyl ether (MTBE) from contaminated water using UV-assisted nano composite materials, Desalin. Water Treat. (2014), doi: 10.1080/19443994.2014.924035

[7] B.S. Tawabini, M. Atieh, M. Mohyeddin, Effect of ultraviolet light on the efficiency of nano photo-catalyst (UV/CNTs/TiO$_2$) composite in removing MTBE from contaminated water, Int. J. Environ. Sci. Dev. 4(2) (2013) 148–151.

[8] C. Baus, F. Sacher, H.J. Brauch, Efficiency of ozonation and AOP for methyl tert-butyl ether (MTBE) removal in water works, Ozone Sci. Eng. 27 (2005) 27–35.

[9] C. Baus, H. Hung, F. Sacher, M. Fleig, H.J. Brauch, MTBE in drinking water production–occurrence and efficiency of treatment technologies, Acta Hydroch. Hydrob. 33 (2005) 118–132.

[10] I. Levchuk, A. Bhatnagar, M. Sillanpää, Overview of technologies for removal of methyl tert-butyl ether (MTBE) from water, Sci. Total Environ. 476–477 (2014) 415–433.

[11] D. Zadaka-Amir, A. Nasser, Sh. Nir, Y.G. Mishael, Removal of methyl tertiary-butyl ether (MTBE) from water by polymer–zeolite composites, Microporous Mesoporous Mater. 151 (2012) 216–222.

[12] L.F. Wieserman, K. Wefer, Surface-modified adsorbent comprising metal oxide/hydroxide particles reacted with one or more perfluorinated organic acids, US Pat. 4,983,566, Aluminum Company of America, 1991.

[13] B. Kasprzyk-Hordern, P. Andrzejewski, A. Dbrowska, K. Czaczyk, J. Nawrocki, MTBE, DIPE, ETBE and TAME degradation in water using perfluorinated phases as catalysts for ozonation process, Appl. Catal., B 51 (2004) 51–66.

[14] B. Kasprzyk, J. Nawrocki, Preliminary results on ozonation enhancement by a perfluorinated bonded alumina phase, Ozone Sci. Eng. 24 (2002) 63–68.

[15] B. Kasprzyk-Hordern, J. Nawrocki, The feasibility of using a perfluorinated bonded alumina phase in the ozonation process, Ozone Sci. Eng. 25 (2003) 185–197.

[16] B. Kasprzyk-Hordern, M. Ziólek, J. Nawrocki, Catalytic ozonation and methods of enhancing molecular ozone reactions in water treatment, Appl. Catal., B 46 (2003) 639–669.

[17] B. Kasprzyk-Hordern, A. Dąbrowska, J. Świetlik, J. Nawrocki, Ozonation enhancement with non-polar bonded Alumina phases, Ozone Sci. Eng. 26 (2004) 367–380.

[18] B. Kasprzyk-Hordern, J. Świetlik, A. Dąbrowska, J. Nawrocki, The application of the perfluorinated bonded alumina phase for natural organic matter catalytic ozonation, Environ. Eng. Sci. 3 (2004) 41–50.

[19] B. Kasprzyk-Hordern, P. Andrzejewski, J. Nawrocki, Catalytic ozonation of gasoline compounds in model and natural water in the presence of perfluorinated Alumina bonded phases, Ozone Sci. Eng. 27 (2005) 301–310.

[20] A. Ebadi, J. Soltan Mohammadzadeh, A. Khudiev, Adsorption of methyl tert-butyl ether on perfluorooctyl alumina adsorbents—High concentration range, Chem. Eng. Technol. 30 (2007) 1666–1673

[21] A. Ebadi, J. Soltan Mohammadzadeh, S. Shafiei, Kinetics of catalytic ozonation of methyl tert-butyl ether in the presence of perfluorooctyl alumina, Chem. Eng. Technol. 32 (2009) 778–788

[22] H.S. Potdar, K.W. Jun, J.W. Bae, S.M. Kim, Y.J. Lee, Synthesis of nano-sized porous γ-alumina powder via a precipitation/digestion route, Appl. Catal., A 321 (2007) 109–116.

[23] J.M. Smith, Chemical Engineering Kinetics, third ed., McGraw-Hill Book Co, New York, NY, 1981.

[24] I. Langmuir, The adsorption of gases on plane surfaces of glass, mica and platinum, J. Am. Chem. Soc. 40 (1918) 1361–1403.

[25] S. Brunauer, P.H. Emmett, E. Teller, Adsorption of gases in multimolecular layers, J. Am. Chem. Soc. 60 (1938) 309–319.

[26] A. Ebadi, J. Soltan Mohammadzadeh, A. Khudiev, What is the correct form of BET isotherm for modeling liquid phase adsorption? Adsorption 15 (2009) 65–73.

[27] K.M. Parida, A.C. Pradhan, J. Das, N. Sahu, Synthesis and characterization of nano-sized porous gamma-alumina by control precipitation method, Mater. Chem. Phys. 113 (2009) 244–248.

[28] S. Wang, X. Li, Sh. Wang, Y. Li, Y. Zhai, Synthesis of γ-alumina via precipitation in ethanol, Mater. Lett. 62 (2008) 3552–3554.

[29] D. Mishra, S. Anand, R.K. Panda, R.P. Das, Preparation of barium hexa-aluminate through a hydrothermal precipitation–calcination route and characterization of intermediate and final products, Mater. Lett. 56 (2002) 873–879.

[30] A.R. Keshavarz, M. Rezaei, F. Yaripour, Preparation of nanocrystalline γ-Al$_2$O$_3$ catalyst using different procedures for methanol dehydration to dimethyl ether, J. Nat. Gas Chem. 20(3) (2011) 334–338.

[31] Ch. Ma, N. Yao, Q. Han, X. Li, Synthesis and application of γ-Al$_2$O$_3$ supported CoRu-based Fischer-Tropsch catalyst, Chem. Eng. J. 191 (2012) 534–540.

[32] R.T. Morrison, R.N. Boyd, Organic Chemistry, fifth ed., Allyn and Bacon, Boston, MA, 1987.

[33] D.Z. Chen, J.X. Zhang, J.M. Chen, Adsorption of methyl tert-butyl ether using granular activated carbon: Equilibrium and kinetic analysis, Int. J. Environ. Sci. Technol. 7(2) (2010) 235–242.

[34] S.K. Ghadiri, R. Nabizadeh, A.H. Mahvi, Sh. Nazmara, S. Nasseri, H. Kazemian, A.R. Mesdaghinia, Methyl tert-butyl ether adsorption on surfactant modified natural zeolites, Iran. J. Environ. Health. Sci. Eng. 7(3) (2010) 241–252.

[35] J. Lu, F. Xu, W. Cai, Adsorption of MTBE on nano zeolite composites of selective supports, Microporous Mesoporous Mater. 108 (2008) 50–55.

[36] H.W. Hung, T.F. Lin, Adsorption of MTBE from contaminated water by carbonaceous resins and mordenite zeolite, J. Hazard. Mater. 135 (2006) 210–217.